Catena 166 (2018) 98–113

Contents lists available at ScienceDirect

Catena

journal homepage: www.elsevier.com/locate/catena

Determination of the shearing behaviour of root-permeated soils with a large-scale direct shear apparatus

A. Yildiz[a,b,c,*], F. Graf[a], C. Rickli[b], S.M. Springman[c]

[a] WSL Institute for Snow and Avalanche Research SLF, Davos Dorf, Switzerland
[b] Swiss Federal Institute for Forest, Snow and Landscape Research WSL, Birmensdorf, Switzerland
[c] Institute for Geotechnical Engineering, ETH Zurich, Zurich, Switzerland

ARTICLE INFO

Keywords:
Shallow landslides
Root reinforcement
Direct shear testing
Dilatancy

ABSTRACT

Soils with roots or root-like inclusions have often been tested in direct shear to quantify the effects of vegetation on the shear strength of soil, and in turn, the stability of slopes. However, a straightforward evaluation of root reinforcement is challenging due to the complex nature of roots, and the dependency of soil behaviour on many factors. An Inclinable Large-scale Direct Shear Apparatus (ILDSA) was built to study the shearing behaviour of root-permeated soils. Planted specimens, consisting of two different sets of species, were prepared with a moraine, sampled from a recent landslide location, and tested in direct shear subsequent to saturation. Relationships of peak stress ratio with dry weight of roots, maximum dilatancy angle and void ratio were investigated to evaluate the behaviour of root-permeated soil. The combined approach, of taking both presence of roots and dilatant behaviour of soil into consideration, results in a more realistic understanding and quantification of the effects of root reinforcement, at least, for laboratory testing of root-permeated soils.

1. Introduction

Soil bioengineering methods, the use of vegetation to prevent superficial erosion or shallow mass movement (Gray and Sotir, 1995), serve as a promising alternative to traditional civil engineering applications to stabilise either man-made or natural slopes against superficial failure. Roots improve the slope stability both mechanically, with roots crossing a potential failure surface (Waldron and Dakessian, 1982), and also hydrologically by evapotranspiration resulting in increased suction in the ground (Blight, 2003; Springman et al., 2003), and to a lesser extent by altering the soil structure (Graf and Frei, 2013; Loades et al., 2010). Roots perform their mechanical reinforcement function by working as tension-carrying fibres that transfer the shear stresses in the soil matrix into tensile resistance via the interface friction along their surface (Gray and Barker, 2004).

Although the physical explanation and interpretation of the mechanism of root reinforcement are simple, a satisfactory way of quantifying and incorporating the biological effects into the conventional slope stability analyses is still a major challenge. This is a considerable disadvantage of soil bioengineering methods (Graf et al., 2009), compared to well-established methods of design and calculation of conventional civil engineering infrastructure, such as retaining walls or soil nailing.

Giadrossich et al. (2017) provided an exhaustive review on the measurement methods of mechanical behaviour of the root-permeated soils. Direct shear tests (Fan and Tsai, 2016; Gonzalez-Ollauri and Mickovski, 2017; Veylon et al., 2015), tensile strength tests on roots (Giadrossich et al., 2016; Leung et al., 2015; Pollen and Simon, 2005), blade penetrometer tests (Meijer et al., 2017a, 2017b) and centrifuge testing (Liang et al., 2017, 2015; Sonnenberg et al., 2010) have been used to assess the vegetation effects on shear strength. The quantification of shear strength of root-permeated soils based on direct shear test results has generally been performed by drawing failure envelopes to Mohr circles in a shear stress (τ) - effective normal stress (σ') diagram either assuming an angle of internal friction equal to that of the fallow soil (Operstein and Frydman, 2000) or without any constraints (Ali and Osman, 2008). The intercept on the shear stress axis is denoted as "*root cohesion*" (c_R) value.

Alternatively, the difference between the peak shear stress of rooted and fallow soils can be recorded as the contribution of roots to the shear strength. These were compared with the c_R values calculated from various models based on measurement of the tensile strength of roots (Comino et al., 2010; Loades et al., 2010; Mickovski et al., 2009); correlated to different root traits (Ghestem et al., 2014) or used in slope stability calculations (Mickovski and van Beek, 2009).

The methods commonly adopted to compare peak shear stress

* Corresponding author at: WSL Institute for Snow and Avalanche Research SLF, Davos Dorf, Switzerland.
E-mail address: anil.yildiz@wsl.ch (A. Yildiz).

https://doi.org/10.1016/j.catena.2018.03.022
Received 20 February 2017; Received in revised form 20 March 2018; Accepted 23 March 2018
Available online 04 April 2018

parameters of root-permeated and fallow soil may both hinder and complicate the quantification of root reinforcement effects. These parameters are dependent on many factors, such as confining pressure, relative density and dilatancy (Das, 2010; Terzaghi et al., 1996), of which the latter presents more difficulty. Dilatancy can be defined as the volume increase of the soil during shearing along a shear surface. Bolton (1986) defines a relative density index (I_R), as follows:

$$I_R = I_D(10 - \ln p') - 1 \quad (1)$$

where I_D is the relative density and p' is the mean effective stress at failure, in kPa. Furthermore, the peak angle of shearing resistance (ϕ_{max}'), the angle of shearing at the critical state with zero dilation (ϕ_{crit}') and maximum dilatancy angle (ψ_{max}) are related to a relative density index under plane strain conditions as defined in Eq. (2).

$$\phi'_{max} - \phi'_{crit} = 0.8\psi_{max} = 5I_R \quad (2)$$

As shown in Eqs. (1) and (2), the peak shear strength parameter is directly dependent on the dilatant behaviour of the soil, which in turn is dependent on the relative density and confining stress. Furthermore, Jewell and Wroth (1987) showed with direct shear tests on reinforced sand that considerably less deformation is required to generate reinforcement forces in dense sand than in loose sand, since the ratio of the principal incremental tensile and compressive strains increases with the dilatancy angle. Therefore, a higher dilatancy angle means higher tensile strains, and in turn, higher tensile forces developing in the roots. It can be expected that dilatancy does not only directly increase the peak shear strength parameters due to interlocking of particles, but amplifies the effects of the roots resulting in even greater changes in peak shear strength.

Some of the stress-displacement, or strain, graphs given in the aforementioned studies exhibited a clear peak and a subsequent reduction in shear stress, which can be attributed to root breakage or pulling out, but it can also be due to particle interlocking and dilatancy. Thus, the comparison of peak shear strength parameters of root-permeated and fallow soil obscures the effects of dilatancy. The increase in the shear strength may not result solely from the contribution of the roots, but from the dilatancy as well. Dilatancy in root-permeated soils has been of interest very recently, although it has been a well-established topic in soil mechanics for many years. Muir Wood et al. (2016) introduced a new modelling framework for root-permeated soils, considering also the dilatancy. Otherwise, quantification of dilatant behaviour of these soils is rare in the literature. Therefore, a laboratory study was conducted with specimens prepared with different combinations of plant species with the following objectives:

i. to investigate the shearing behaviour of root-permeated soil specimens exhibiting dilatancy under saturated conditions,
ii. to propose a combined method of dilatancy and root biomass to explain the shear strength of root-permeated soils.

2. Materials & methods

2.1. Soil

The soil used to prepare the samples was collected from the moraine of a subalpine landslide location, Hexenruebi in Dallenwil, in canton Nidwalden, Switzerland. The area is a gully, where biological and technical stabilization measures have been taken and investigated over three decades by the Swiss Federal Institute for Forest, Snow and Landscape Research (WSL) (e.g. Burri et al., 2009).

The soil was dried in an oven at 105 °C for 24 h and subsequently sieved to discard the particles having a size > 20 mm. The particle size distribution, as illustrated in Fig. 1, was obtained from two

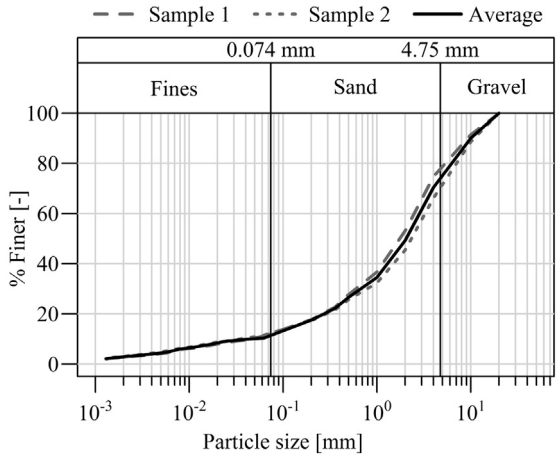

Fig. 1. Particle size distribution of two samples of Hexenruebi soil from the main batch obtained by wet sieving and hydrometer method.

representative samples from the main batch by wet sieving in combination with the hydrometer method (ASTM D 422, 2007). The particle sizes separating the clay, sand and gravel were chosen according to ASTM D 2487 (2006). The liquid and plastic limits were determined by using a Casagrande tool and applying the thread-rolling method, respectively (ASTM D 4318, 2010). The liquid limit was 13.3%, while the plastic limit was calculated to be 16.8%. As the plastic limit was found to be higher than the liquid limit, the soil is classified as non-plastic (Allen, 1942; White, 1949). The specific gravity was determined by using a water pycnometer (ASTM D 854, 2010), and was calculated as 2.69. Soil was classified as SP-SM according to the Unified Soil Classification System (USCS).

2.2. Sample preparation

The preparation of a planted specimen consists of several steps, including the compaction of soil in the shear boxes, as well as previous plant breeding and growth. First of all, oven-dried Hexenruebi soil (D_{max} < 20 mm) is filled into wooden split boxes (500 × 500 × 400 mm) and compacted in three layers up to a height of 300 mm by applying 15 blows per layer using a 4.5 kg compaction rammer with a drop height of 460 mm. The compaction was performed at heights of 120, 220 and 300 mm from the bottom of the box, in order that the compaction zones did not coincide with the pre-defined failure surface.

Plant breeding starts by filling germination pots of 100-mm-diameter with a peat-sand mixture of high water retention capacity. Seeds from each species are obtained from the WSL seedbank, distributed randomly on the surface of the mixture in the pots and covered with an extra 1–2 mm thick layer of peat-sand mixture. After a 6–8 week growth period of individual plants in the germination pots, four individual plants from each species are transferred carefully to eight defined spots that are distributed on the surface of the soil in the shear boxes. Each spot had a total of 12 individual plants (4 individual plants of 3 species each) for the HLP6 set, while there were 24 individual plants (4 individual plants of 6 species each) in each planting spot for the HHP6 set. This resulted in a total number of 96 plants and 192 for HLP6 and HHP6, respectively. No intervention was made during the plant growth. The approximate locations are shown schematically in Fig. 2a, and on a planted shear box in Fig. 2b.

Germination pots and shear boxes are kept under controlled temperature and humidity in a climate chamber, where the daylight conditions are 24 °C, 70% humidity and 2400 lx light intensity between

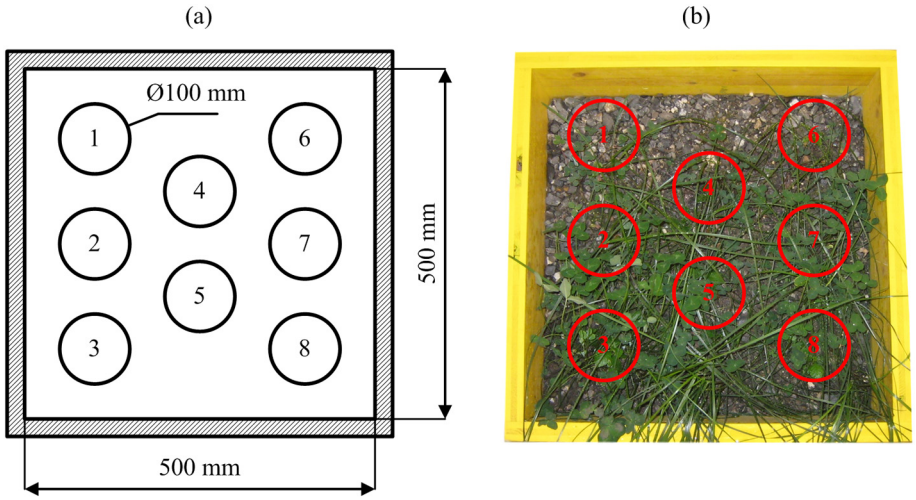

Fig. 2. Schematic drawing of the planting spots 1 to 8 (a) and approximate locations of planting spots at the end of growth period for the first specimen of HLP6 group, HLP6_S1_1 (b).

05:00 and 20:00, and 17 °C and 55% humidity with no light during the night. All the specimens are maintained inclined at 30° from the horizontal in order to simulate the natural growth of roots on a vegetated slope.

2.3. Experimental design

Two different categories of plants, namely woody plants (*Alnus incana* (L.) Moench, *Salix appendiculata* Vill.) and non-woody plants (*Achillea millefolium* L., *Anthyllis vulneraria* L., *Poa pratensis* L., *Trifolium pratense* L.), were used in order to investigate the shearing behaviour of root-permeated soils. The experimental design consists of two groups of specimens: The first group of 9 specimens, HLP6 (6-month-old specimens with low level plant diversity), was prepared with Hexenruebi soil, and planted with low level plant diversity, namely *Alnus incana*, *Trifolium pratense*, and *Poa pratensis*. The second group of 6 specimens, HHP6 (6-month-old specimens with high level plant diversity), was prepared with Hexenruebi soil, and planted with high level plant diversity, consisting of *Salix appendiculata*, *Achillea millefolium*, *Anthyllis vulneraria* in addition to the aforementioned species in the low level plant diversity configuration.

All of the species used in both groups were nursed in the way described in the section above, except *Salix appendiculata*, of which 1-year-old cuttings were used in the specimens within the HHP6 group. In addition to the main group names HLP6 and HHP6, each specimen is also characterised based on the normal stress level (_S1, _S2 and _S3) and the number of repetitions (_1, _2 and _3). For example, HLP6_S1_1 stands for the first specimen tested at the lowest normal stress within the HLP6 group.

2.4. Inclinable Large-scale Direct Shear Apparatus (ILDSA)

The Inclinable Large-scale Direct Shear Apparatus (ILDSA) was built in the WSL Institute for Snow and Avalanche Research SLF in order to test root-permeated soil specimens in direct shear. It offers a possibility to span the gap between results obtained from small-scale planted soil specimens and the stability calculation of entire slopes with vegetation.

Shibuya et al. (1997) describes three types of direct shear apparatuses with respect to the configuration of the upper half of the shear box and the loading platen. The ILDSA design was based on Shibuya et al.'s (1997) recommendations of an optimal shear box with a fixed upper half and a non-rotating loading platen. The applied normal load can be measured in this configuration, either conventionally with an external load cell between the loading platen and the load application system, or it can be measured at the bottom of the shear box.

Fig. 3 is a 3D sketch of the ILDSA, showing the main components, namely the normal load and shear force application setups, shear box, the measuring and data logging system, the base plate, loading platen, counterweight and main frame. A linear actuator (Thomson T 60) is coupled with a synchronous servomotor (Beckhoff AM3032-0C40-0000) to serve as a linear driving unit to apply a normal load up to 10 kN on a steel plate. The loading platen is fixed against rotation, but allowed to move freely in the axis perpendicular to the surface of the specimen. The shear force is applied with a similar linear driving unit, consisting of a linear actuator (Thomson T 90) coupled with a synchronous servomotor (Beckhoff AM3042-0E40-0000). A maximum shear force of 20 kN can be applied at a constant rate of shear displacement as low as 0.01 mm/min.

The apparatus is equipped with a variety of sensors to monitor the status and/or movement of the different components. Data from the sensors are recorded with a PLC data logger system. The normal load and the shear force are measured during testing with a load cell for each (HBM C2). The normal load is regulated throughout the shearing by controlling the displacement of the loading piston of the linear driving unit. The movement of the loading platen in the axis perpendicular to the surface of the specimen is measured with a laser displacement sensor (Baumer OADM 13U6475/S35A) and the inclination of the loading platen is monitored with a 2D inclination sensor (Micronor MR401-3). A potentiometric linear transducer (Megatron MMS33) is placed on the linear driving unit of the shear load application system to measure the shear displacement. The shear box rests on a steel base plate, and two load cells at the back and at the front are embedded into the base plate to measure the normal load transferred to the bottom of the box. A steel plate supports the shear box in the front, and a load cell is mounted into the plate to monitor the force that has been applied to the plate by the box. The apparatus is also equipped with a metal plate to prevent loss of soil from the top half of the shear box during shearing.

2.5. Direct shear testing

All of the specimens were sheared to failure in the ILDSA after a total growth period of 6 months, including the time in the germination

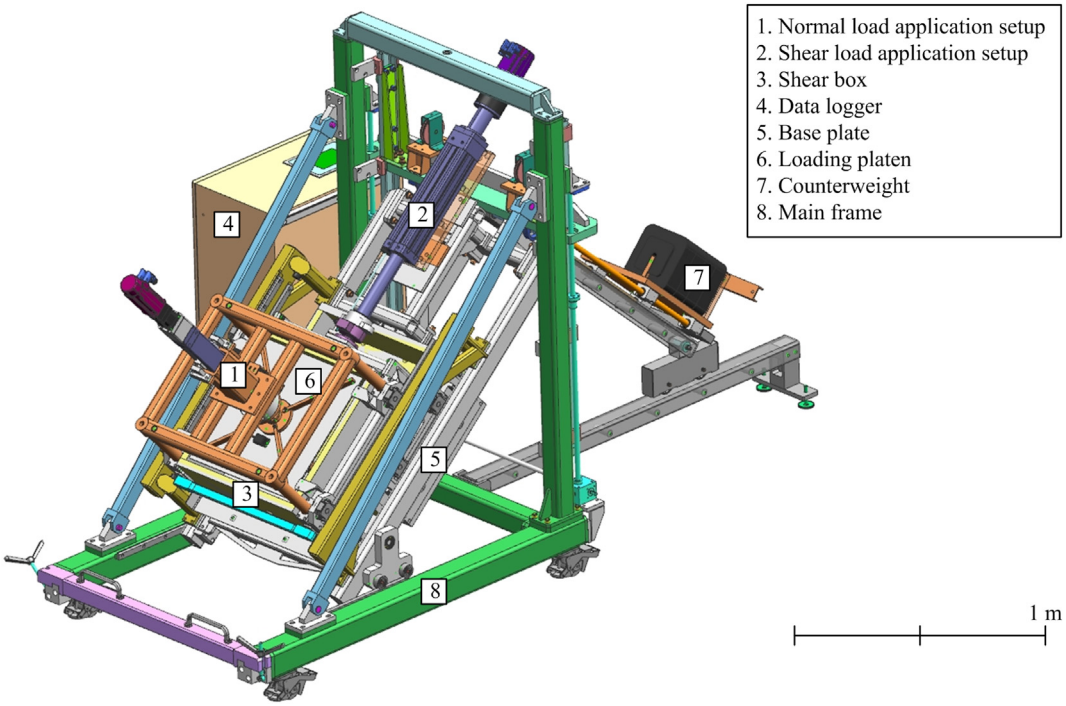

Fig. 3. 3D drawing of the Inclinable Large-scale Direct Shear Apparatus (ILDSA).

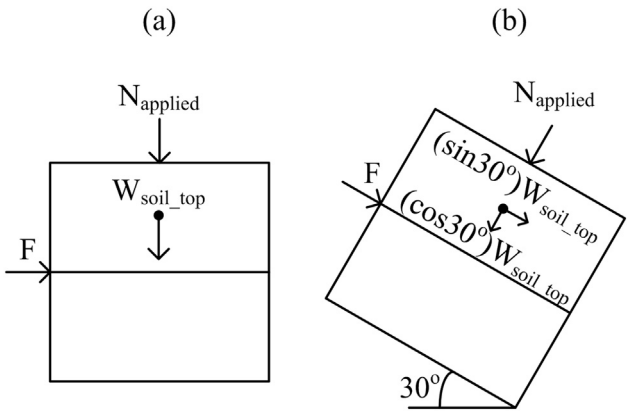

Fig. 4. Forces acting on the specimens in the shear box for tests performed horizontally (a) and inclined by 30° (b).

pots. The above ground biomass (AGB) was cut prior to testing, and the dry weight of shoots of each species was determined. To simulate the loss of strength due to saturation (Springman et al., 2003), which can happen after a heavy rainfall period in nature, the specimens were saturated with a rainfall simulator, as described by Germann et al. (2007). Artificial rainfall was applied at a constant intensity of 100 mm/h for 60 min, followed by a 30-minute break, and further rainfall for 30 min. Tensiometers (UMS T5x) were installed close to the shear surface, and monitored continuously to obtain the matric suction during the saturation and shearing process. Suctions were reduced as close to 0 kPa as possible.

Direct shear tests were conducted at an inclination of 30° from the horizontal axis at a constant rate of shear displacement of 1 mm/min parallel to the slope, up to a maximum shear displacement of 190 mm, and under three different applied normal loads: 1500, 2750 and 4000 N. The normal load levels were chosen to be comparable to typical depths of shallow landslides (Rickli and Graf, 2009; Springman et al., 2003). Subsequent to shearing, the specimens were dug out to unearth the below ground biomass. The roots were washed and separated to quantify the roots in the top and bottom halves of the shear box, and their dry weight was determined.

2.6. Data analyses

Data analyses include the determination of the saturated unit weight, void ratio, strength parameters and dilatancy calculations. Saturated unit weight, expressed as kN/m^3, is calculated by dividing the weight of saturated specimens by the nominal volume of the specimen. The distance between the top of the box and the soil surface is consistently measured at nine points as a 3 × 3 grid distributed over the surface and the specimen height is determined by taking the average of these nine measurements. Volume is calculated by multiplying the three dimensions of the specimen. Saturated unit weight can also be expressed as shown in Eq. (3), where γ_{sat} is the saturated unit weight, G_s is the specific gravity, γ_w is the unit weight of water (taken as 9.81 kN/m^3), and e is the void ratio.

$$\gamma_{sat} = \frac{(G_s + e)\gamma_w}{1 + e} \quad (3)$$

The void ratio of each specimen after the completion of irrigation and before shearing is obtained by back-calculation, as shown in Eq. (4), derived from Eq. (3).

$$e = \frac{G_s\gamma_w - \gamma_{sat}}{\gamma_{sat} - \gamma_w} \quad (4)$$

The height of the soil above the shear surface in a large-scale direct shear test is substantially higher than that in a small-scale direct shear test. As the overburden pressure corresponds to 12 to 35% of the applied normal stress in this study, the weight of the soil above the shear surface was taken into consideration in the calculation of normal stress on the shear surface. Fig. 4a and b depict the forces acting on the

specimens for tests conducted horizontally and inclined at 30° from the horizontal axis, respectively. The total normal force acting on the element (N) for a horizontal test is equal to the sum of the weight of the soil above the shear element (W_{soil_top}) and the applied normal load ($N_{applied}$), whereas N is equal to the sum of the applied normal load and the component of the weight of the soil above the shear surface acting perpendicular to the shear surface, as shown in Eq. (5).

A correction to take the mechanical friction of the apparatus into consideration is applied, as described in Yildiz et al. (2015). Furthermore, a second correction to the measured shear force is applied to take the soil-to-metal interface friction into account, the details of the correction is given in Appendix A. The total shear force acting on the element (T) is equal to the corrected shear force (F) for the tests conducted horizontally. However, the component of the weight of the soil acting along the shear surface is added to the applied shear force for the inclined tests, as shown in Eq. (6).

$$N = N_{applied} + (\cos 30^{\circ}) W_{soil.top} \tag{5}$$

$$T = F + (\sin 30^{\circ}) W_{soil.top} \tag{6}$$

As the matric suction was brought as close as possible to 0 kPa to ensure saturation, the uplifting force due to pore pressure (U) was also assumed to be 0 kN, and all the analyses were done using the effective stress concept, so that $N' = N - U = N$. By employing effective stress analysis, a mobilised friction angle (ϕ_{mob}') and a mobilised stress ratio, $(\tau/\sigma')_{mob}$, can be calculated, as described in Eqs. (7) and (8), respectively.

$$\phi'_{mob} = \tan^{-1}(T/N') \tag{7}$$

$$(\tau/\sigma')_{mob} = (T/N') \tag{8}$$

The maximum value of the corrected shear force between the initial stages of shearing displacement up to 80 mm, $(F_C)_{max}$, and the parallel component of the weight of the soil above the shear surface are added and divided by the corrected cross-sectional area at the displacement where $(F_C)_{max}$ occurs to determine the peak shear stress (τ_{max}). Later stages of shearing displacement are discarded since the primary assumptions made in calculating the stresses acting on the shear plane are no longer valid due to large relative displacements between the top and bottom parts of the box. Normal stress at peak is obtained by adding the applied normal load at the displacement of peak shear force and the perpendicular component of the weight of the soil above the shear surface and dividing this value by the same corrected cross-sectional area used in the calculation of the peak shear stress. The peak stress ratio, $(\tau/\sigma')_{peak}$, is defined as the ratio of the peak shear stress and the normal stress at peak.

The vertical displacement was measured with a laser displacement sensor only at the centre point, and recorded at every 100 ms. Therefore, a smoothing process with a local polynomial regression was applied in order to filter the noise from the data, using the "lpridge" function in the software R 3.1.3 (R Core Team, 2017), which was used for all statistical analyses including correlation, pairwise tests and linear regression. The change in the normal displacement (dy) was calculated at 2 mm steps of change in the shear displacement (dx). The rate of dilation (dy/dx) was defined and the dilation angle (ψ) was calculated, as shown in Eq. (9).

$$\psi(^{\circ}) = \tan^{-1}\frac{dy}{dx} \tag{9}$$

Fig. 5a shows the actual measurements of the data of normal displacement with noise and smoothed curves for the first specimen of HLP6 group and Fig. 5b shows the change in dilatancy angle with shear displacement. The maximum value of the dilatancy angle is defined as the maximum dilatancy angle (ψ_{max}).

3. Results

3.1. Vegetation

Table 1 shows the dry weight of the woody, non-woody and total AGB of both the low level and high level plant diversity sets. The minimum, maximum and average values are also given. The dry weight of the woody AGB was substantially lower than that of the non-woody AGB for all specimens. Both the woody and non-woody plants in HLP6 specimens yielded less AGB, on average, than those in HHP6 specimens. Non-woody AGB was correlated positively and significantly with the total AGB of HLP6 ($R^2 = 0.89$, $p < 0.001$), HHP6 ($R^2 = 0.84$, $p < 0.01$), and all specimens ($R^2 = 0.89$, $p < 0.001$). There were positive and significant correlations of the dry weight of woody AGB with that of the non-woody AGB ($R^2 = 0.40$, $p < 0.05$) and total AGB ($R^2 = 0.73$, $p < 0.001$) if all the specimens were considered, but not individually for different groups.

In terms of below ground biomass, HHP6 had a higher amount of roots, on average, than HLP6. The comparison of the values of the roots in the bottom half of the box and in the top half of the box shows that a limited amount of roots managed to pass through the shear surface. However, there is a significant correlation ($R^2 = 0.30$, $p < 0.05$) between these two parameters. Investigating the relationships between the dry weight of AGB and roots yielded a positive and significant ($R^2 = 0.80$, $p < 0.001$) correlation, as illustrated in Fig. 6., The woody AGB is correlated significantly and positively with both the amount of roots in the top ($R^2 = 0.87$, $p < 0.001$) and bottom ($R^2 = 0.32$, $p < 0.05$) halves of the shear box When the woody and non-woody plant types are compared with the amount of roots in the top and bottom halves of the shear box. However, the dry weight of non-woody AGB is only correlated with the roots in the top half of the box ($R^2 = 0.55$, $p < 0.001$).

3.2. Direct shear tests

The corrected shear force – shear displacement graphs are shown in Figs. B.1 and B.2 for all the specimens within the HLP6 and HHP6 groups, respectively. All the specimens in HLP6 and HHP6 exhibit dilatant behaviour subsequent to an initial contractive response, as shown in the dilatancy angle – shear displacement graphs in Figs. C.1 and C.2. However, not all the specimens showed a distinct peak shear force value followed by a decrease in shear force. Furthermore, the peak stress ratios, as defined in Section 2.6, do not necessarily coincide with the points of shear displacements where the maximum dilatancy angles occur.

The shear strength of root-permeated specimens tested in this study was found to be exclusively frictional, as illustrated in Fig. 7. The failure envelopes of the planted and unplanted specimens prepared with a moraine from the same study site, and tested in isotropic consolidated undrained triaxial compression by Graf et al. (2009) are also given in Fig. 7. HHP6_S1_2, shown with the hallow triangle in the figure, laid below the failure envelope of the unplanted specimens, yielding a peak friction angle even smaller than the friction angle at critical state, which cannot be expected to occur. Further inspection of the experiment showed that the initial mobilisation of the forces was delayed, and the maximum shear force was reduced excessively after the friction correction had been performed. As a result, the data point of HHP6_S1_2 was kept in figures, but excluded from the statistical analyses of shear strength parameters.

Unconstrained regressions of peak failure envelopes with a weighting factor based on the dry weight of roots of each specimen

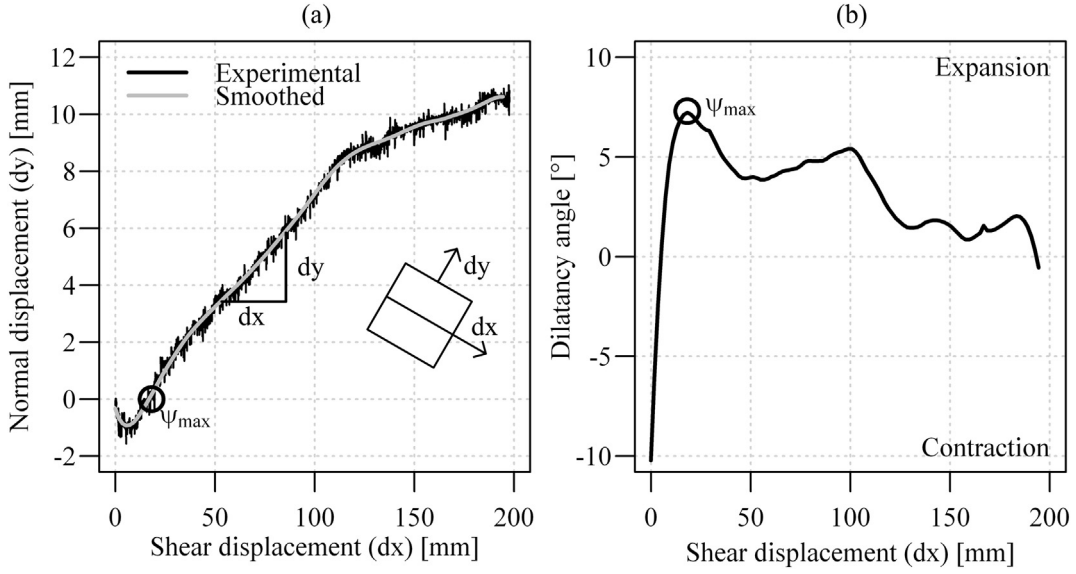

Fig. 5. Normal-shear displacement (a) and dilatancy angle-shear displacement (b) curves of the first specimen of the HLP6 group, HLP6_S1_1. The black solid line in Fig. 5a shows the experimental measurements of the normal displacement, while the gray solid line is the smoothed curve. Positive values of normal displacement (dy) and dilatancy angle indicate expansion, while the negative values of normal displacement (dy) and dilatancy angle indicate contraction. The circles in both graphs show the position of maximum dilatancy angle (ψ_{max}).

yielded a negative intercept of −0.48 on the y-axis, as a negative intercept is not physically meaningful and the value is rather low, a constraint of 0 intercept was introduced (Merrien-Soukatchoff and Omraci, 2004). A generalised linear model with 0 intercept and the aforementioned weighting factor yielded a peak friction angle of 48.3°. Correlations between shear strength parameters and vegetation parameters are shown in Table 2. Peak stress ratio values are plotted against the dry weight of all roots for each specimen in Fig. 8a. HHP6 yielded lower values than HLP6, despite the higher amount of roots present in the boxes.

Two different relationships of peak stress ratio and dry weight of roots are observed for each group. Firstly, peak stress ratios of the specimens within HLP6 group are significantly and positively correlated with the dry weight of all roots ($R^2 = 0.72$, $p < 0.01$) and roots in the top half of the shear box ($R^2 = 0.72$, $p < 0.01$). No correlation was found between the peak stress ratios and the dry weight of the roots in the bottom half of the shear box (see Table 2). Secondly, peak stress ratios of specimens within HHP6 had positive, however insignificant, correlations with the roots in the bottom half of the shear box, the roots in the top half of the shear box, and all roots. If all the specimens are considered for the linear regression analyses, there are no significant correlations between the peak stress ratios and the dry weight of all roots, or roots in the top half of the shear box or those in the bottom half of the shear box. However, there were significant negative correlations of the peak stress ratios with the woody AGB ($R^2 = -0.40$, $p < 0.05$).

Fig. 8b shows the relationship between the peak stress ratio and the maximum dilatancy angle. A positive and significant correlation exists for HLP6 ($R^2 = 0.75$, $p < 0.01$), but not for HHP6. A linear regression model for these two parameters, considering all specimens, yielded a positive and significant correlation ($R^2 = 0.67$, $p < 0.001$). Void ratio

Table 1
Dry weight of woody, non-woody and total above ground biomass (AGB); and roots in the bottom half, and the top half of the shear box; and total amount of roots. For each group, (_S1, _S2, _S3) and (_1, _2, _3) stand for the three different applied normal load and repetitions.

Specimen	Woody AGB [g]	Non-woody AGB [g]	Total AGB [g]	Roots in bottom box [g]	Roots in top box [g]	Total roots [g]
HLP6_S1_1	1.2	17.0	18.2	0.2	5.2	5.4
HLP6_S1_2	1.5	14.0	15.5	0.4	5.4	5.8
HLP6_S1_3	1.4	18.9	20.3	0.5	3.9	4.4
HLP6_S2_1	0.6	19.3	19.9	0.4	7.0	7.4
HLP6_S2_2	1.1	16.5	17.6	0.5	7.2	7.7
HLP6_S2_3	4.5	12.1	16.6	0.4	7.2	7.6
HLP6_S3_1	0.9	18.2	19.1	0.3	8.4	8.7
HLP6_S3_2	0.7	14.8	15.5	0.3	4.8	5.1
HLP6_S3_3	1.3	8.5	9.8	0.3	4.2	4.5
Min.–Max.	0.6–4.5	8.5–19.3	9.8–20.3	0.2–0.5	3.9–8.4	4.4–8.7
Average	1.5	15.5	16.9	0.4	5.9	6.3
HHP6_S1_1	14.3	27.3	41.6	0.1	20.3	20.4
HHP6_S1_2	5.1	33.6	38.7	0.7	12.1	12.8
HHP6_S2_1	11.6	30.0	41.6	2.2	15.8	18.0
HHP6_S2_2	8.9	26.9	35.8	0.2	12.7	12.9
HHP6_S3_1	13.3	34.5	47.8	1.5	25.2	26.7
HHP6_S3_2	10.5	12.6	23.1	1.7	15.0	16.7
Min.–Max.	5.1–14.3	12.6–34.5	23.1–47.8	0.1–2.2	12.1–25.2	12.8–26.7
Average	10.6	27.5	38.1	1.1	16.9	17.9

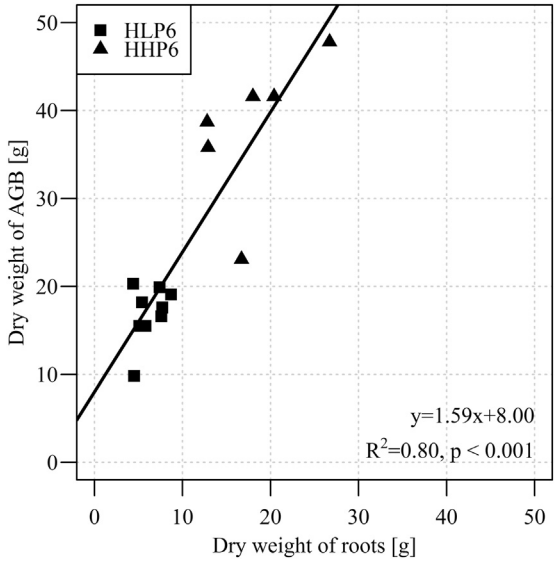

Fig. 6. Relationship of dry weight of above ground biomass (AGB) and roots for all specimens.

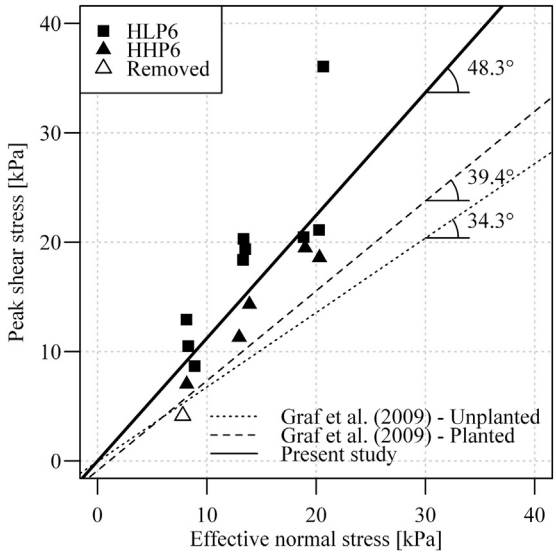

Fig. 7. Shear stress – effective normal stress graph of all experiments.

Table 2
R-squared values of the correlations and significance of the shear strength and vegetation parameters.

Relationships	HLP6	HHP6	All
$(\tau/\sigma')_{peak}$ vs. roots in bottom	–	–	–
$(\tau/\sigma')_{peak}$ vs. roots in top	0.72**	–	–
$(\tau/\sigma')_{peak}$ vs. all roots	0.72**	–	–
$(\tau/\sigma')_{peak}$ vs. woody AGB	–	–	−0.40*
$(\tau/\sigma')_{peak}$ vs. non-woody AGB	–	–	–
$(\tau/\sigma')_{peak}$ vs. total AGB	–	–	–
$(\tau/\sigma')_{peak}$ vs. ψ_{max}	0.75**	–	0.67***
$(\tau/\sigma')_{peak}$ vs. e	–	–	−0.52**
ψ_{max} vs. e	–	–	−0.47**

* $p < 0.05$.
** $p < 0.01$.
*** $p < 0.001$.

is correlated negatively with the peak stress ratio ($R^2 = -0.52$, $p < 0.01$) and maximum dilatancy angle ($R^2 = -0.47$, $p < 0.01$) for all specimens, as shown in Fig. 8c and d, and it was correlated positively with the total AGB ($R^2 = 0.29$, $p < 0.05$).

The transfer of the applied normal load ($N_{applied}$) to the shear surface, and thus to the bottom of the shear box, is directly affected by the dilatant behaviour of the soil. The ILDSA is equipped with four load cells, embedded in the plate that the shear box stands on, to measure the transferred normal load to the bottom of the box ($N_{transferred}$). A second stress ratio was calculated with the transferred normal load and the maximum value of corrected shear force up to a shear displacement of 80 mm, and it was denoted as transferred stress ratio, $(\tau/\sigma')_{transferred}$. Fig. 9 shows the relationship between the peak stress ratio, $(\tau/\sigma')_{peak}$, and the transferred stress ratio, $(\tau/\sigma')_{transferred}$. The dashed line in the figure indicates the points where the two stress ratios are equal. It was found that the peak stress ratios calculated with the transferred normal load were 5% lower than those calculated with the applied and regulated normal load.

4. Discussion

The significant difference in the dry weight of total AGB between the two groups of specimens is due to the greater number of species in high level plant diversity and presence of 1-year-old *Salix appendiculata* cuttings, which already produced more AGB due to the greater age. The average dry weight of total AGB was 16.9 g and 38.1 g for HLP6 and HHP6, respectively (see Table 1). If the dry weight of *Salix appendiculata* is excluded from the total AGB, the average dry weight of total AGB reduces to 27.9 g for HHP6. Hence nearly one third of the total AGB was produced by *Salix appendiculata* cuttings. The rest of the difference in AGB is attributed to the presence of the higher number of species. Common non-woody plants between the two different groups of specimens, namely *Poa pratensis* and *Trifolium pratense*, produced less AGB in specimens of the HHP6 group. However, the greater dry weight of the remaining non-woody plants resulted in the difference between the groups.

Observations during plant growth showed that the non-woody plants used in the specimens developed faster than the woody plants and, therefore, had a considerable advantage in the competition for water and nutrients. Correspondingly, they produced more biomass within the same growth period than their woody competitors. The relationship of AGB and roots, shown in Fig. 6, suggests that AGB was an appropriate indicator of root growth in this study.

Further inspection of the AGB-root relationship provided the aforementioned correlations of the woody AGB with roots in the bottom half of the shear box and of non-woody AGB with roots in the top half of the shear box. These correlations, supported with the post-test observations, give a hint on the growth patterns of different root types, i.e. shallow-rooting non-woody plants vs. woody plants with thicker and penetrating roots. Although it was intended to create similar root growth conditions to a vegetated slope, accumulation of water in the downslope part of the boxes could not be prevented with the current setup. Post-test observations also indicated dominant root growth in the direction of downslope, which differs from root growth observed on slopes in the field (Shrestha et al., 2000)

Graf et al. (2009) used a moraine from the same study site, and performed isotropic consolidated undrained triaxial compression tests on samples planted with *Alnus incana*. The slopes of the failure envelopes of the unplanted and planted specimens, shown in Fig. 7, yielded friction angles of 34.3° and 39.4°, respectively. Both specimen types yielded slightly negative intercepts. Similar to the failure envelope of the specimens of this study, Graf et al. (2009) found no additional

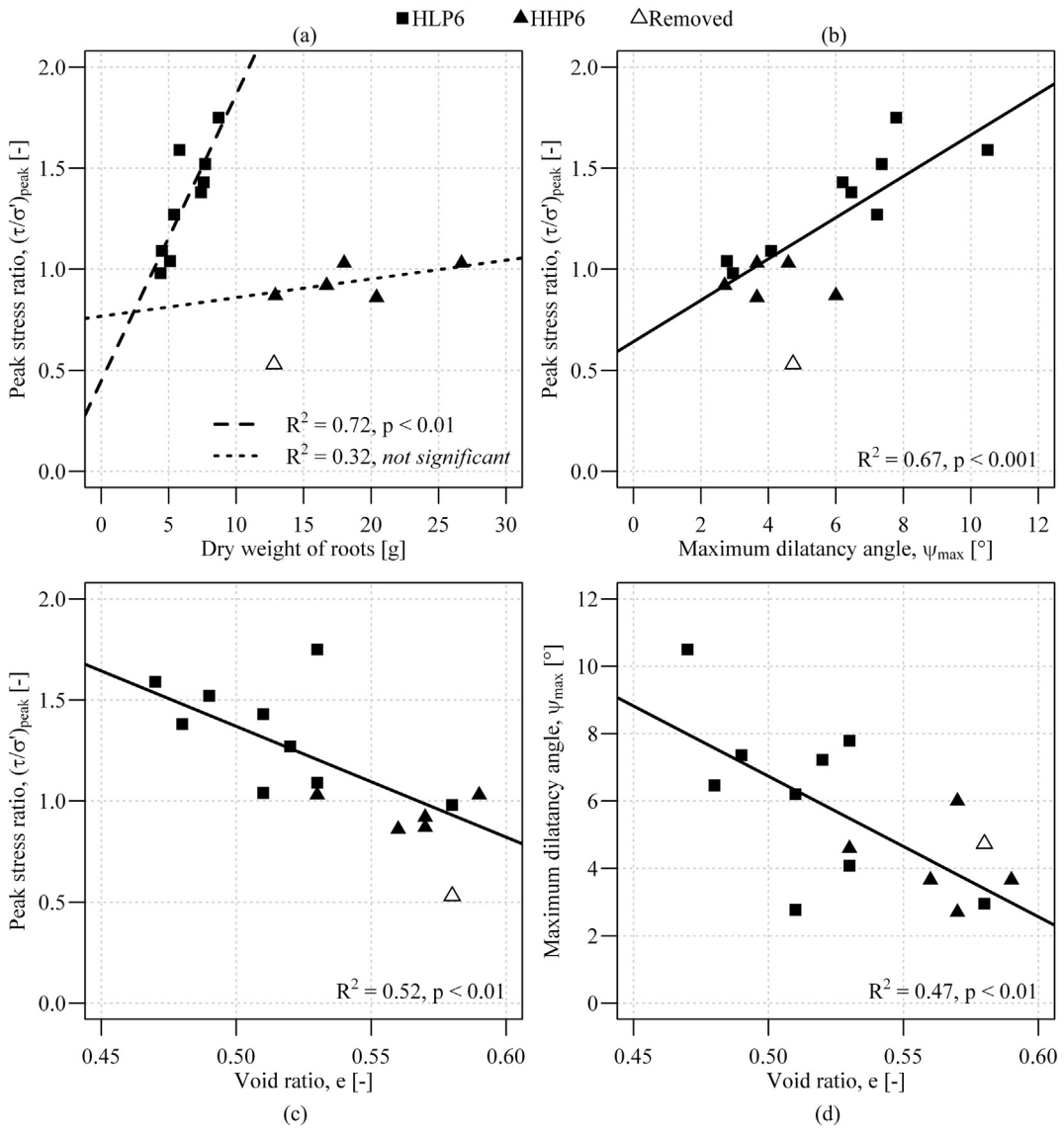

Fig. 8. Relationships of peak stress ratio and dry weight of roots (a), maximum dilatancy angle (b), void ratio (c); and the relationship between the maximum dilatancy angle and void ratio (d). The solid lines show the linear regressions for all experiments.

cohesion term due to presence of roots and the contribution of roots attributed to an increase in the peak angle of internal friction.

The friction angle values obtained from Graf et al. (2009) for the loosely compacted fallow and planted specimens are the friction angles at phase transformation. This angle corresponds to the angle of internal friction at critical state, ϕ_{crit}', (Frei, 2009), which is independent of confining pressure and density (Schofield and Wroth, 1968). Bolton (1986) formed his empirical formula based on the assumption of an equal ϕ_{crit}' for both plane strain and triaxial stress states, before adding 3 I_R (triaxial) or 5 I_R (plane strain) to obtain ϕ_{max}'. It was also shown experimentally that there was no difference in between these states (Schanz and Vermeer, 1996), provided that the soil remained the same and there were no particle size – apparatus dimension effects. Therefore, the values from Graf et al. (2009) were taken as a basis for comparison as the densities of the specimens tested in this study varied highly.

ϕ_{crit}' of the planted specimens tested in this study was determined by plotting the peak friction angle against the maximum dilatancy angle over a range of densities, and reading the intercept value at the zero dilatancy. Fig. 10 shows the relationship of the peak friction angle and maximum dilatancy angle for all experiments. The intercept on the y-axis at zero dilatancy gives a value of 36.9°, which can be considered as ϕ_{crit}' of the soil tested in ILDSA and it is between the ϕ_{crit}' values of the unplanted and planted specimens from Graf et al. (2009). It should be noted that the maximum particle size in this study is greater than that of Graf et al. (2009), which can result in an increase in ϕ_{crit}' (Simoni and Houlsby, 2006). Springman et al. (2003) also showed a ϕ_{crit}' from direct shear tests in the field 2° higher than that from triaxial tests. As there was no control of the maximum size in the field conditions, the particle size – apparatus interactions played a role in the variation of ϕ_{crit}'.

Graf et al. (2009) showed a difference of 5° in the friction angles of planted and fallow soil specimens, and concluded that this difference results from the presence of the roots. A substantially higher peak friction angle was observed in this study, however considering this value only as the contribution of roots can be misleading, as the specimens tested exhibited dilatant behaviour. The variation between the

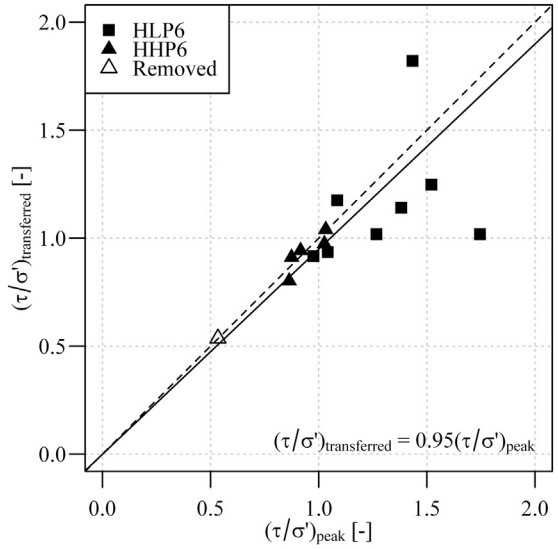

Fig. 9. Comparison of peak stress ratio calculated with transferred normal load, $(\tau/\sigma')_{transferred}$, and that calculated with applied normal load, $(\tau/\sigma')_{peak}$. The dashed line indicates where both parameters are equal, and the solid line indicates the relationship derived from the experiments in this study.

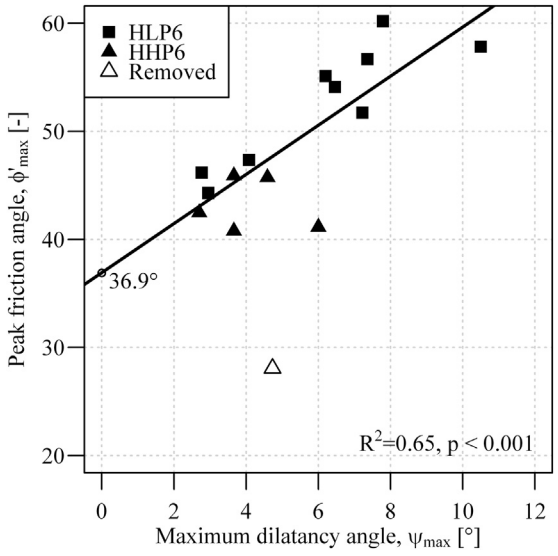

Fig. 10. Peak friction angle – maximum dilatancy angle graph of all experiments.

peak angle of internal friction found in this study and those determined in Graf et al. (2009) can be attributed to the differences in maximum particle size and confining pressure, i.e. the increase in confining pressure leads to decreased peak angle of internal friction angle (Bishop, 1971; Bolton, 1986). The initial normal stresses applied in the large-scale direct shear tests in this study were ranging between 6 and 16 kPa, whereas Graf et al. (2009) performed triaxial tests with confining pressures ranging between 50 and 100 kPa. Therefore, it is expected that dilatancy will be lower, with reduced values of peak angle of internal friction angle at higher confining pressures.

Despite the same compaction effort being applied during the sample preparation, and the same maintenance during the plant growth period, specimens within the HLP6 group had, on average, lower void ratio, hence a higher maximum dilatancy angle was mobilised than for those

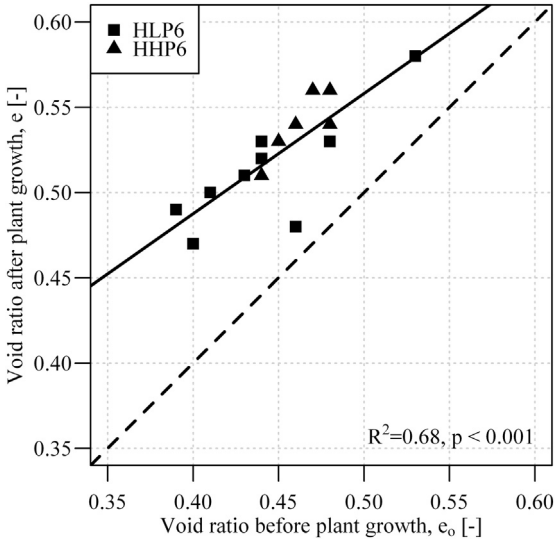

Fig. 11. Relationship of the void ratios of all specimens before (e_o) and after (e) the plant growth. Dashed line indicates where both values are equal.

within the HHP6 group. Mitigation of volume change due to root growth can be shown with the differences in the void ratios of the specimens for HLP6 group. Void ratio after the sample preparation in dry conditions (e_o) prior to planting of the shear boxes can be back-calculated as shown in Eq. (10) modified from the formula of the dry unit weight of soil (γ_{dry}).

$$e_o = \frac{G_s \gamma_w}{\gamma_{dry}} - 1 \tag{10}$$

Fig. 11 illustrates the void ratios of the specimens before (e_o) and after (e) the plant growth. The mean and standard deviation values of void ratios before plant growth were 0.44 ± 0.04 for the HLP6 group and 0.46 ± 0.02 for the HHP6 group. There were no significant differences between the two groups of specimens, but there was a positive and significant (R^2 = 0.68, p < 0.001) relationship between the void ratios before and after the plant growth for all specimens.

Bolton (1986) relates the maximum dilatancy angle with the relative density, and expresses a positive correlation between these two

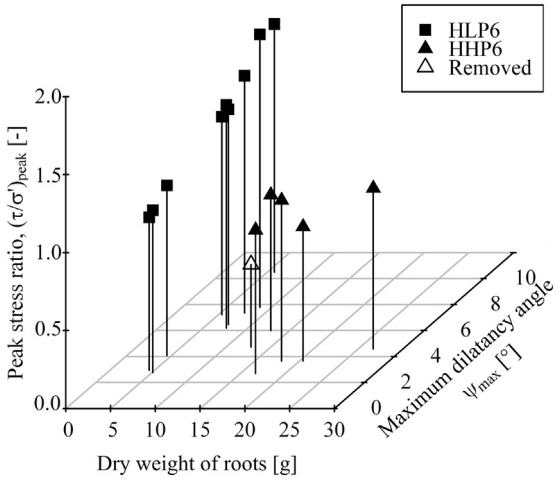

Fig. 12. 3D graph of peak stress ratio, dry weight of roots and maximum dilatancy angle for all experiments.

parameters, as shown in Eq. (6). As relative density is negatively correlated with the void ratio (Terzaghi et al., 1996), the negative correlation between the maximum dilatancy angle and the void ratio, which was found based on the experimental data, explains the higher maximum dilatancy angle in HLP6 specimens. The observed higher void ratios can be due to the thicker roots of the woody plants and the higher amount of roots in HHP6 specimens. Lower peak stress ratios were observed in HHP6 specimens compared to HLP6 due to the higher void ratio, and the maximum dilatancy angle, and despite the greater amount of roots. Although the root biomass is not a representative parameter of root morphology or architecture, it was linked directly with shear strength of root-permeated soils for specimens tested in direct shear (Saifuddin et al., 2015) and with vane shear testing (Micheli and Kirchner, 2002).

Although in the case of dense granular soils, the maximum dilation rate (i.e. maximum dilatancy angle) is achieved at the strain corresponding to the maximum shear stress (Terzaghi et al., 1996), the aforementioned differences in the strains where the peak stress ratio and the maximum dilatancy angle occur can be attributed to the differences in strain uptake of roots and soil (Simon and Pollen, 2004). In other words, when the soil reaches its peak strength and maximum dilatancy angle, roots do not necessarily need to be extended to mobilise their maximum tensile strength. A peculiarity observed in the dilatant behaviour of root-permeated soils tested in this study can also explain the reduced post-peak strength loss. Dilatancy angle – shear displacement graphs presented in Figs. C.1 and C.2 show a decrease after the maximum dilatancy angle is reached, however a renewed increase in dilatancy angle can be observed subsequent to the decrease. The difference is more noticeable in the HLP6 group than the HHP6, which can be due to higher dilatancy angles observed in the first group.

The range of void ratios observed in the specimens resulted in a range of maximum dilatancy angles. Two different correlations between the peak stress ratio and amount of roots, both positive but significant only for HLP6, were observed for the two different groups of plant diversity (see Fig. 8a and d). It should also be noted, again, that dilatancy was positively correlated with the peak stress ratio (see Fig. 8b).

A series of multiple linear regression analyses was performed considering the effects of roots on the peak stress ratio, and the contribution of the dilatancy to the peak shear strength parameters. Fig. 12 shows a 3D graph of peak stress ratio, dry weight of roots and maximum dilatancy angle. The multiple linear regression for HLP6 provided a higher R^2 value of 0.96 and positive and significant correlations with the dry weight of all roots and maximum dilatancy angle, which explains more of the variation in the data. However, it did not give a significant relationship for HHP6. Furthermore, the dilatancy was negatively correlated with the peak stress ratio. A multiple linear regression on all experiments yielded a significant relationship with an R^2 value of 0.71. Dilatancy had a positive, but roots a negative effect on the peak stress ratio, due to the lower peak stress ratios observed in specimens within the HHP6 group.

The combined effect of roots and dilatancy explains the measured peak stress ratios from all experiments, which was not possible if only the amount of roots in the shear box was considered. An analogy to frozen sand can be used to explain the significance of the multiple linear regression with root reinforcement and dilatancy. Ting et al. (1983) described the components of the strength of frozen sand based on the volume fraction of sand. Higher volume fractions of sand emphasise soil strength, in which inter-particle friction plays a more important role. On the one hand, the HLP6 group had fewer roots and lower void ratios on average, which can be considered as a high volume fraction of soil similar to the concept of frozen sand, and, in return, a higher number of particle-to-particle contacts. Therefore, the physical mechanism of soil strength and dilatancy play a principal role, and there was less variance when the peak stress ratio was related to roots and dilatancy. On the other hand, HHP6 had more roots and higher void ratios on average. A lower volume fraction of soil results in a lower number of particle-to-particle contacts, which yielded, in the end, higher variance and non-significant results based on statistical evidence.

In addition to the investigations of the root reinforcement, the results of the direct shear tests on root-permeated soil specimens performed within the current study (see Fig. 9), indicate an overestimation of the stress ratio as well, if it is calculated based on the applied normal load, when the top half is fixed against vertical movement. This is due to the frictional forces developing on the inner faces of the side walls of the shear box when the soil is dilatant. Findings from this study, in terms of the stress ratios calculated with the applied and transferred normal loads, validate the experimental findings of Shibuya et al. (1997) and Wu et al. (2008), as well as the numerical findings of Liu (2006).

5. Conclusions

The results of direct shear tests performed with a recently constructed inclinable large-scale direct apparatus on root-permeated soils are presented herein. The shearing behaviour of root-permeated soil was explained via the relationships of peak stress ratio, maximum dilatancy angle, root biomass, and void ratio. It was found that root growth altered the initial void ratio, although the samples were prepared in dry condition with the same compaction effort. It was also shown that the dilatancy combines with the effects of root reinforcement on the shear strength parameters below a threshold value of root biomass. The combination of maximum dilatancy angle and the dry weight of roots explained the most of the variance in peak stress ratio. To conclude, quantification of root reinforcement effects on the shear strength requires the consideration of soil-related mechanisms and parameters, in particular void ratio, dilatancy, and biological parameters.

Acknowledgements

This study is funded by the Swiss National Science Foundation within the framework of the National Research Programme “Sustainable Use of Soil as a Resource” (NRP 68, Project no. 143122). The authors would like to express their sincere gratitude to Andreas Tröger (†), Marco Collet and Andreas Moser with their help for the construction and the maintenance of the apparatus, and to Peter Schweizer for his support and guidance with the gardening.

Appendix A. Method of correction for friction on metal plate

Frictional force developing on the metal plate (F_{plate}), shown in Fig. A.1, was calculated as follows:

$$F_{plate} = R \times \tan\delta \quad (A.1)$$

where R is the total vertical reaction force on the metal plate and δ is the interface friction angle between the soil and metal plate. It is assumed that the applied normal stress and the pressure exerted by the soil above the shear plane are homogeneously distributed over the shear zone. The total reaction force on the metal plate can be calculated as follows:

$$R = \frac{N_{applied} + \cos 30 \times W_{soil,top}}{500 \times 500} \times (dx \times 500) \tag{A.2}$$

where dx is the shear displacement.

The interface friction angle between the soil and metal plate is assumed to be 2/3 of the internal friction angle of the soil. The value of the critical state friction angle of the soil from the same area, which was 34.3°, is taken from Graf et al. (2009).

Thus, for each point of shear displacement, the frictional force developing on the metal plate can be calculated from Eqs. (A.1) and (A.2) as follows:

$$F_{plate} = \frac{N_{applied} + \cos 30 \times W_{soil,top}}{500 \times 500} \times (dx \times 500) \times \tan\left(\frac{2}{3} \times 34.3\right)$$

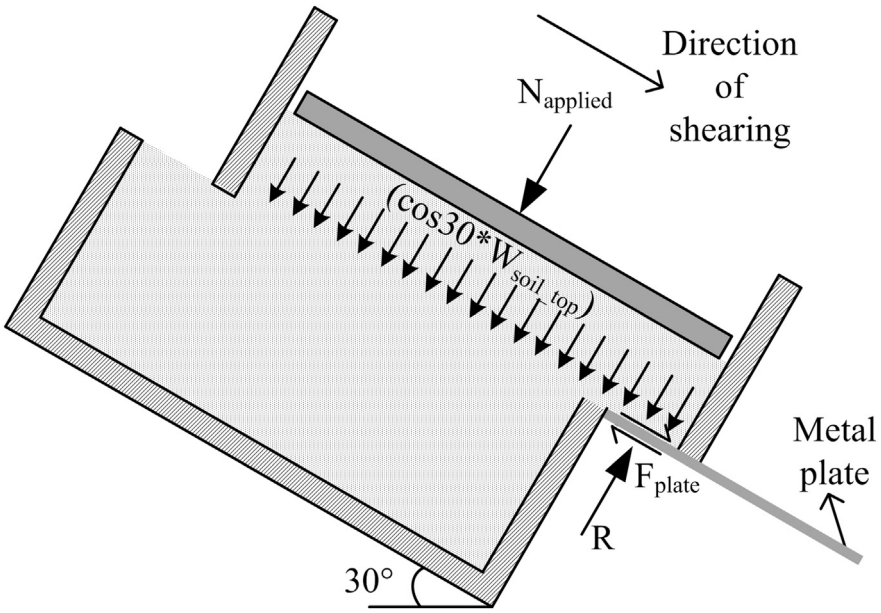

Fig. A.1. Calculation of correction for friction on metal plate.

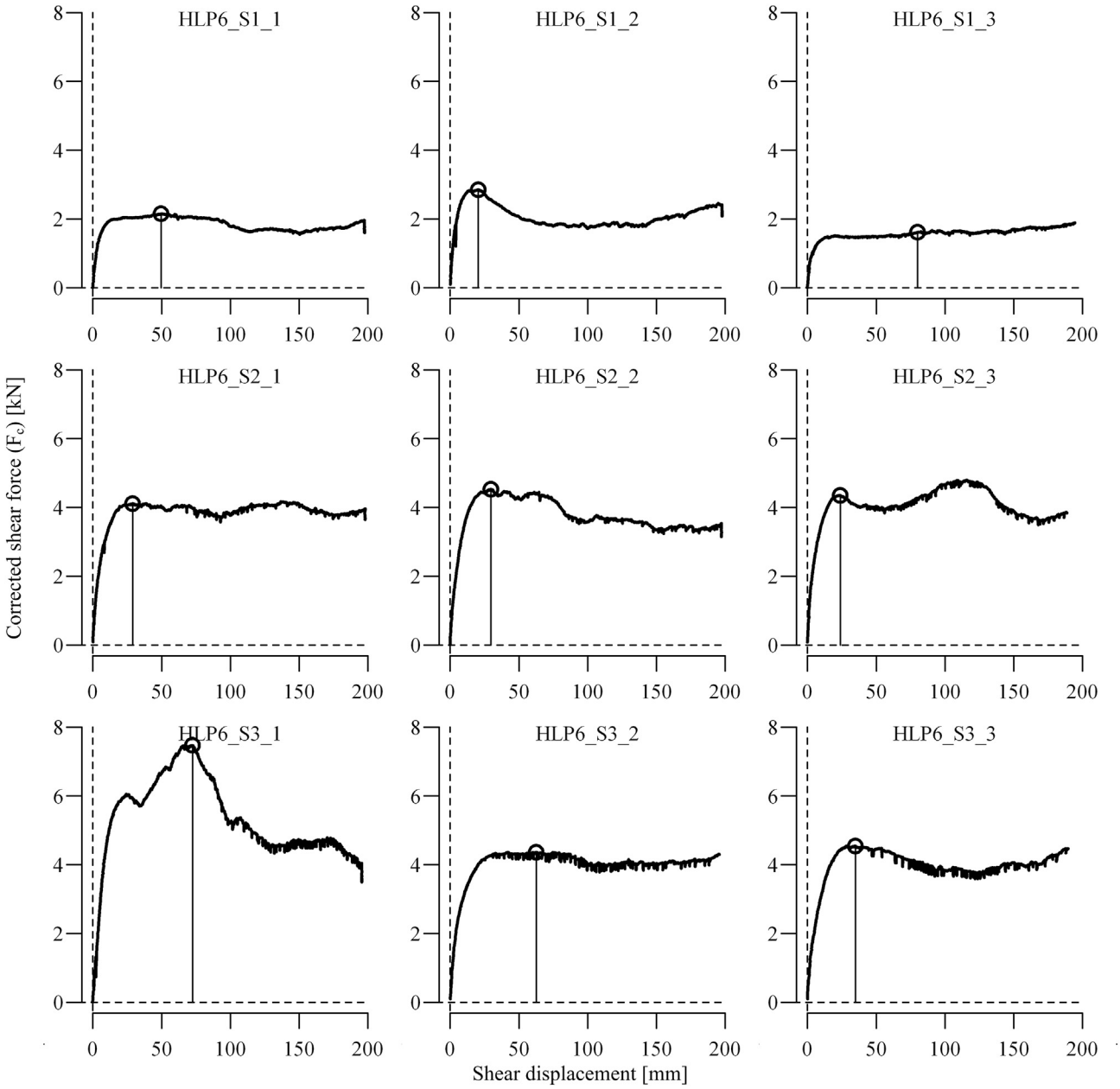

Fig. B.1. Corrected shear force – shear displacement graphs for HLP6 specimens. Circles mark the peak value of F_c in the first 80 mm of shear displacement. The values after 80 mm shear displacement are plotted here for reference.

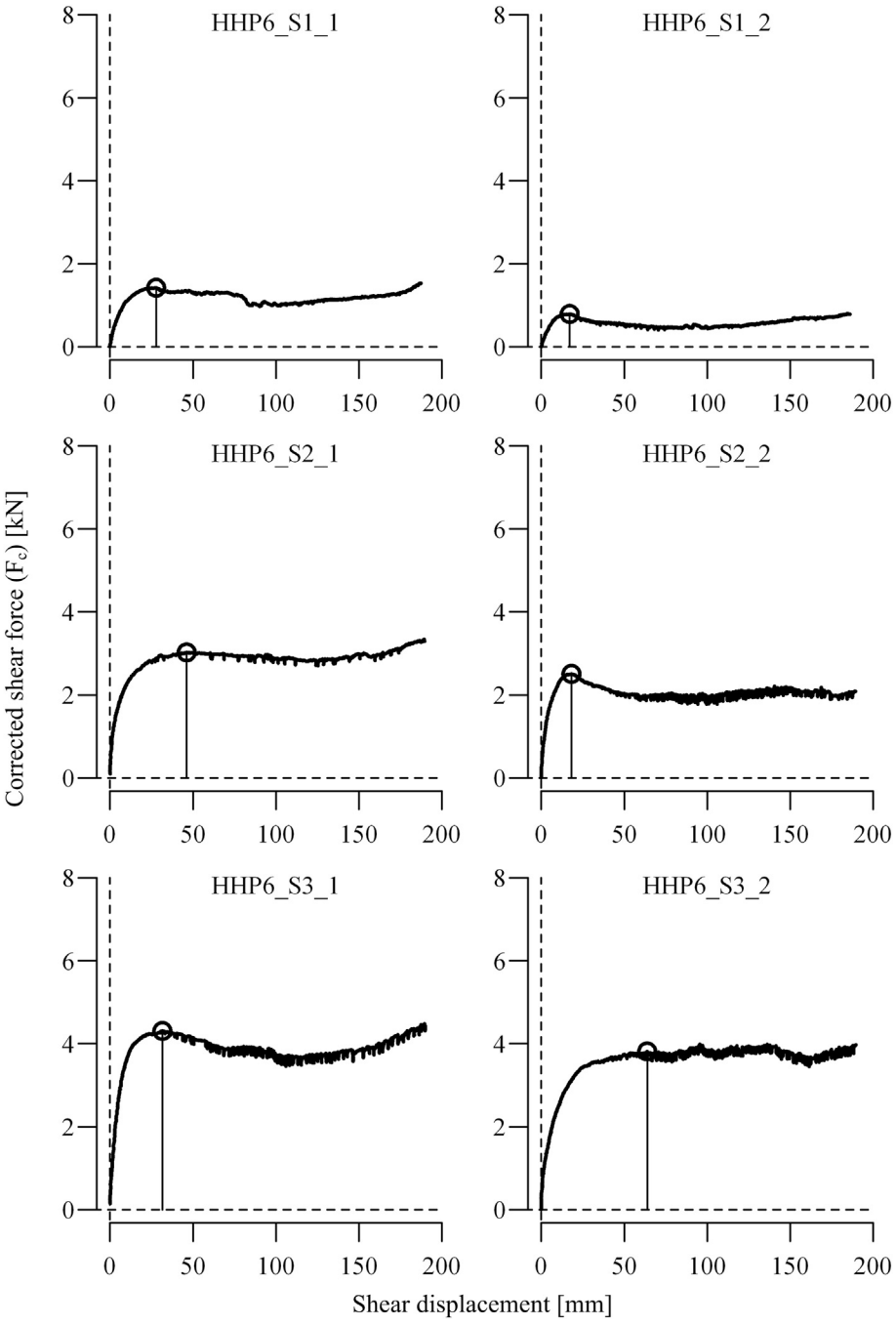

Fig. B.2. Corrected shear force – shear displacement graphs for HHP6 specimens. Circles mark the peak value of F_c in the first 80 mm of shear displacement. The values after 80 mm shear displacement are plotted here for reference.

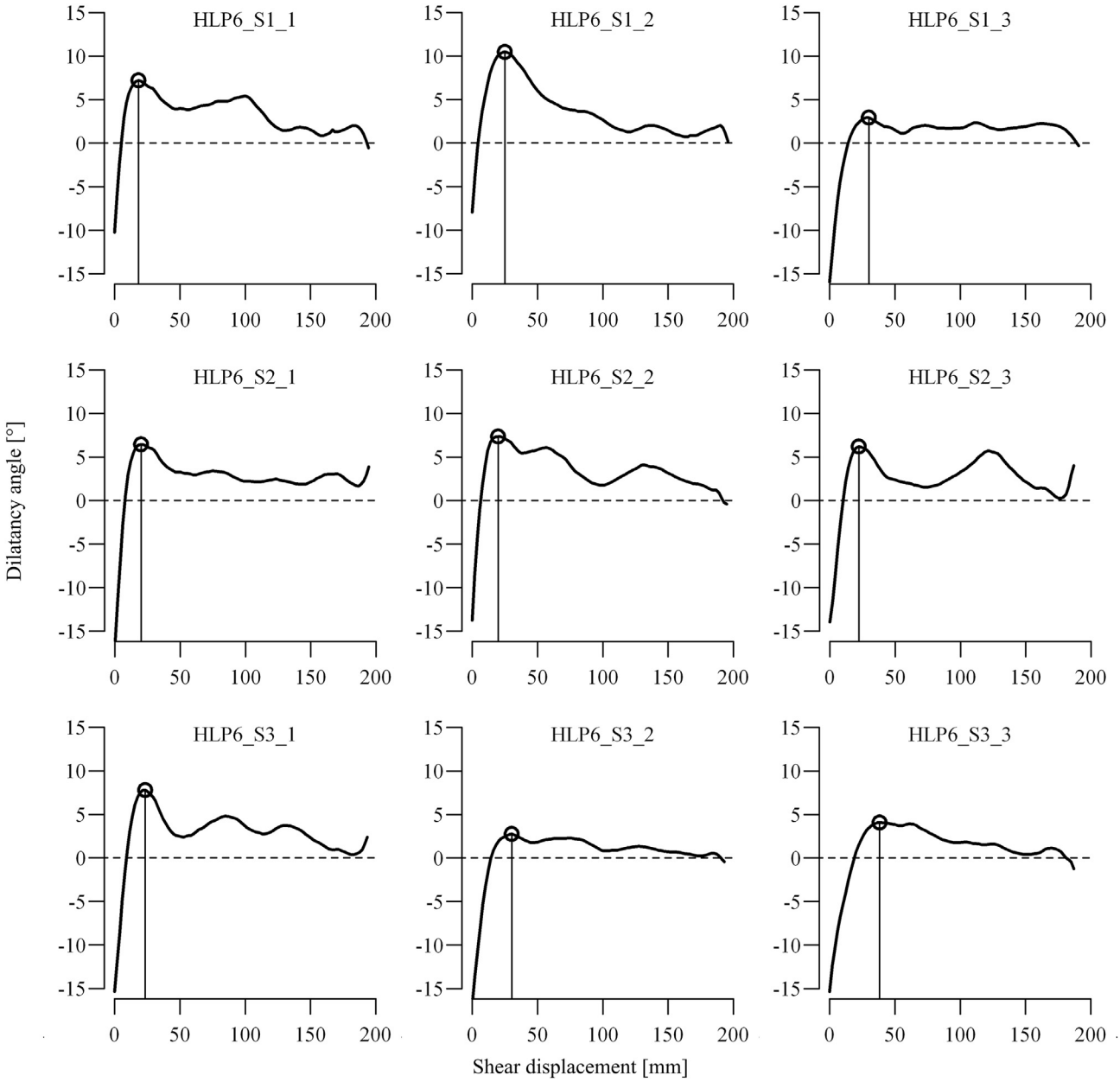

Fig. C.1. Dilatancy angle – shear displacement graphs for HLP6 specimens.

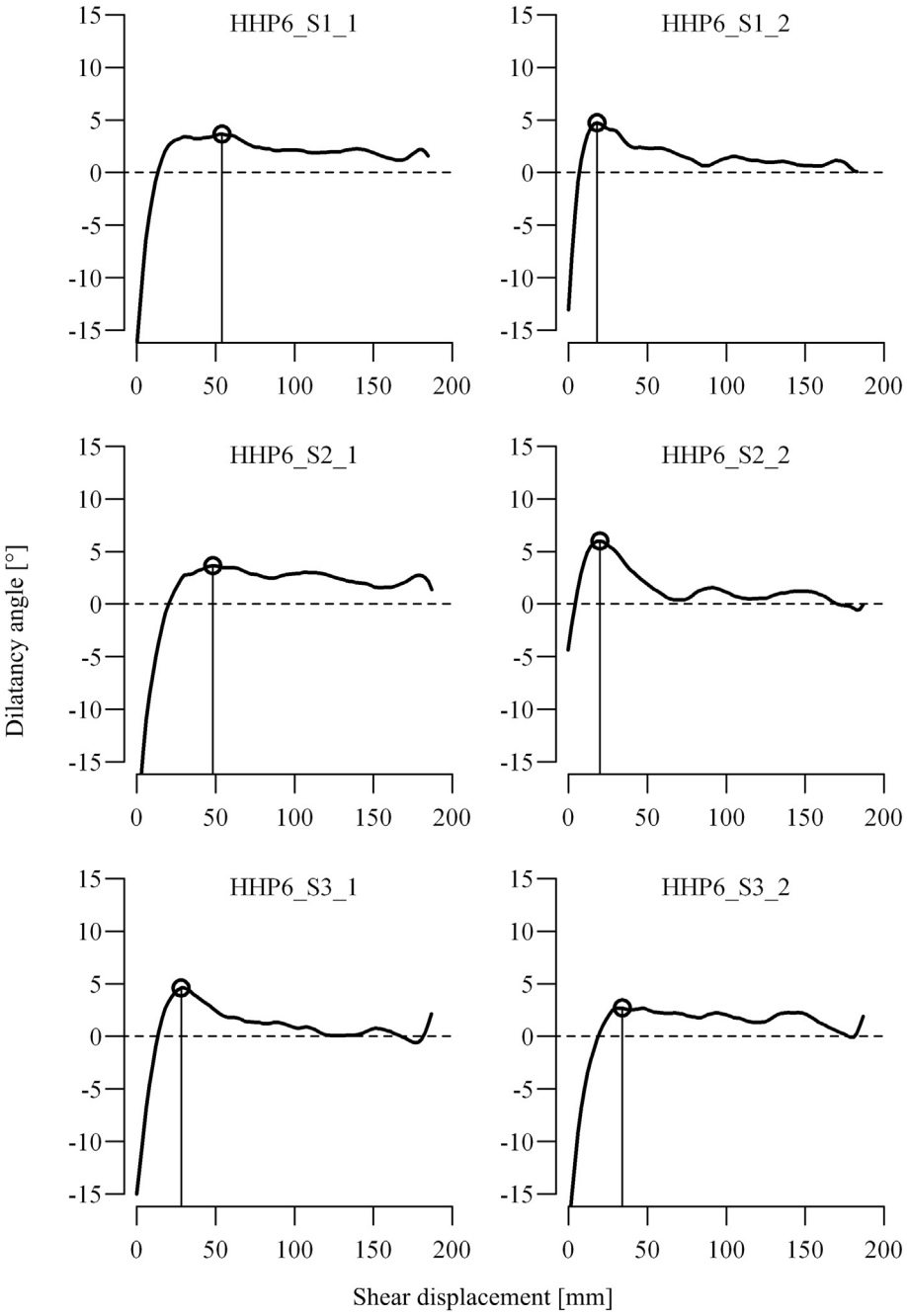

Fig. C.2. Dilatancy angle – shear displacement graphs for HHP6 specimens.

References

Ali, F.H., Osman, N., 2008. Shear strength of a soil containing vegetation roots. Soils Found. 48, 587–596. http://dx.doi.org/10.3208/sandf.48.587.

Allen, H., 1942. Classification of soils and control procedures used in construction of embankments. Public Roads 22, 263–265.

ASTM D 2487, 2006. Standard Practice for Classification of Soils for Engineering Purposes (Unified Soil Classification System). ASTM Internationalhttp://dx.doi.org/10.1520/D2487-11.

ASTM D 422, 2007. Standard Test Method for Particle - Size Analysis of Soils. ASTM Internationalhttp://dx.doi.org/10.1520/D0422-63R07E02.

ASTM D 4318, 2010. Standard Test Methods for Liquid Limit, Plastic Limit, and Plasticity Index of Soils. ASTM Internationalhttp://dx.doi.org/10.1520/D4318-10E01.

ASTM D 854, 2010. Standard Test Methods for Specific Gravity of Soil Solids by Water Pycnometer. ASTM Internationalhttp://dx.doi.org/10.1520/D0854-14.

Bishop, A.W., 1971. Shear strength parameters for undisturbed and remoulded soil specimens. In: Parry, R.H.G. (Ed.), Proceedings of the Roscoe Memorial Symposium. Cambridge, pp. 3–58.

Blight, G.E., 2003. The vadose zone soil-water balance and transpiration rates of vegetation. Géotechnique 53, 55–64. http://dx.doi.org/10.1680/geot.2003.53.1.55.

Bolton, M.D., 1986. The strength and dilatancy of sands. Géotechnique 36, 65–78. http://dx.doi.org/10.1680/geot.1986.36.1.65.

Burri, K., Graf, F., Böll, A., 2009. Revegetation measures improve soil aggregate stability: a case study of a landslide area in Central Switzerland. For. Snow Landsc. Res. 82, 45–60.

Comino, E., Marengo, P., Rolli, V., 2010. Root reinforcement effect of different grass species: a comparison between experimental and models results. Soil Tillage Res. 110, 60–68. http://dx.doi.org/10.1016/j.still.2010.06.006.

Das, B.M., 2010. Principles of Geotechnical Engineering, 7th ed. Cengage Learning, Stamford, USA.

Fan, C.C., Tsai, M.H., 2016. Spatial distribution of plant root forces in root-permeated soils subject to shear. Soil Tillage Res. 156, 1–15. http://dx.doi.org/10.1016/j.still.2015.09.016.

Frei, M., 2009. Validation of a New Approach to Determine Vegetation Effects on Superficial Soil Movements.

Germann, P., Helbling, A., Vadilonga, T., 2007. Rivulet approach to rates of preferential infiltration. Vadose Zo. J. 6, 207. http://dx.doi.org/10.2136/vzj2006.0115.
Ghestem, M., Veylon, G., Bernard, A., Vanel, Q., Stokes, A., 2014. Influence of plant root system morphology and architectural traits on soil shear resistance. Plant Soil 377, 43–61. http://dx.doi.org/10.1007/s11104-012-1572-1.
Giadrossich, F., Cohen, D., Schwarz, M., Seddaiu, G., Contran, N., Lubino, M., Valdés-Rodrígguez, O.A., Niedda, M., 2016. Modeling bio-engineering traits of *Jatropha curcas* L. Ecol. Eng. 89, 40–48. http://dx.doi.org/10.1016/j.ecoleng.2016.01.005.
Giadrossich, F., Schwarz, M., Cohen, D., Cislaghi, A., Vergani, C., Hubble, T., Phillips, C., Stokes, A., 2017. Methods to measure the mechanical behaviour of tree roots: a review. Ecol. Eng. 109, 256–271. http://dx.doi.org/10.1016/j.ecoleng.2017.08.032.
Gonzalez-Ollauri, A., Mickovski, S.B., 2017. Plant-soil reinforcement response under different soil hydrological regimes. Geoderma 285, 141–150. http://dx.doi.org/10.1016/j.geoderma.2016.10.002.
Graf, F., Frei, M., 2013. Soil aggregate stability related to soil density, root length, and mycorrhiza using site-specific *Alnus incana* and *Melanogaster variegatus* s.l. Ecol. Eng. 57, 314–323. http://dx.doi.org/10.1016/j.ecoleng.2013.04.037.
Graf, F., Frei, M., Boll, A., 2009. Effects of vegetation on the angle of internal friction of a moraine. For. Snow Landsc. Res. 82, 61–77.
Gray, D.H., Barker, D., 2004. Root-soil mechanics and interactions. Riparian Veg. Fluv. Geomorphol. 113–123. http://dx.doi.org/10.1029/008WSA09.
Gray, D.H., Sotir, R.B., 1995. Biotechnical stabilization of steepened slopes. In: Prepared for Transportation Research Board 74th Annual Meeting.
Jewell, R.A., Wroth, C.P., 1987. Direct shear tests on reinforced sand. Géotechnique 37, 53–68. http://dx.doi.org/10.1680/geot.1987.37.1.53.
Leung, F.T.Y., Yan, W.M., Hau, B.C.H., Tham, L.G., 2015. Root Systems of Native Shrubs and Trees in Hong Kong and Their Effects on Enhancing Slope Stability. http://dx.doi.org/10.1016/j.catena.2014.10.018.
Liang, T., Knappett, J.A., Duckett, N., 2015. Modelling the seismic performance of rooted slopes from individual root–soil interaction to global slope behaviour. Géotechnique 65, 995–1009. http://dx.doi.org/10.1680/jgeot.14.P.207.
Liang, T., Bengough, A.G., Knappett, J.A., Muirwood, D., Loades, K.W., Hallett, P.D., Boldrin, D., Leung, A.K., Meijer, G.J., 2017. Scaling of the reinforcement of soil slopes by living plants in a geotechnical centrifuge. Ecol. Eng. 109, 207–227. http://dx.doi.org/10.1016/j.ecoleng.2017.06.067.
Liu, S.H., 2006. Simulating a direct shear box test by DEM. Can. Geotech. J. 43, 155–168. http://dx.doi.org/10.1139/t05-097.
Loades, K.W., Bengough, A.G., Bransby, M.F., Hallett, P.D., 2010. Planting density influence on fibrous root reinforcement of soils. Ecol. Eng. 36, 276–284. http://dx.doi.org/10.1016/j.ecoleng.2009.02.005.
Meijer, G.J., Bengough, G., Knappett, J., Loades, K., Nicoll, B., 2017a. In situ root identification through blade penetrometer testing – part 2: field testing. Géotechnique 1–12. http://dx.doi.org/10.1680/jgeot.16.P.204.
Meijer, G.J., Bengough, G., Knappett, J., Loades, K., Nicoll, B., Mukov, I., Zhang, M., 2017b. In situ root identification through blade penetrometer testing – part 1: interpretative models and laboratory testing. Géotechnique 1–17. http://dx.doi.org/10.1680/jgeot.16.P.203.
Merrien-Soukatchoff, V., Omraci, K., 2004. Various assessments of the characteristic values of soil cohesion and friction angle: application to New Caledonian laterite. In: Engineering Geology for Infrastructure Planning in Europe: A European Perspective, pp. 144–152.
Micheli, E.R., Kirchner, J.W., 2002. Effects of wet meadow riparian vegetation on streambank erosion. 2. Measurements of vegetated bank strength and consequences for failure mechanics. Earth Surf. Process. Landforms 27, 687–697. http://dx.doi.org/10.1002/esp.340.
Mickovski, S.B., van Beek, L.P.H., 2009. Root morphology and effects on soil reinforcement and slope stability of young vetiver (*Vetiveria zizanioides*) plants grown in semi-arid climate. Plant Soil 324, 43–56. http://dx.doi.org/10.1007/s11104-009-0130-y.
Mickovski, S.B., Hallett, P.D., Bransby, M.F., Davies, M.C.R., Sonnenberg, R., Bengough, A.G., 2009. Mechanical reinforcement of soil by willow roots: impacts of root properties and root failure mechanism. Soil Sci. Soc. Am. J. 73, 1276. http://dx.doi.org/10.2136/sssaj2008.0172.
Muir Wood, D., Diambra, A., Ibraim, E., 2016. Fibres and soils: a route towards modelling of root-soil systems. Soils Found. 56, 765–778. http://dx.doi.org/10.1016/j.sandf.2016.08.003.
Operstein, V., Frydman, S., 2000. The influence of vegetation on soil strength. Proc. Inst. Civ. Eng. - Gr. Improv. 4, 81–89. http://dx.doi.org/10.1680/grim.2000.4.2.81.
Pollen, N., Simon, A., 2005. Estimating the mechanical effects of riparian vegetation on stream bank stability using a fiber bundle model. Water Resour. Res. 41, 1–11. http://dx.doi.org/10.1029/2004WR003801.
R Core Team, 2017. R: A Language and Environment for Statistical Computing. R Foundation for Statistical Computing, Vienna, Austria.
Rickli, C., Graf, F., 2009. Effects of forests on shallow landslides – case studies in Switzerland. For. Snow Landsc. Res. 82 (1), 33–44.
Saifuddin, M., Osman, N., Motior Rahman, M., Boyce, A.N., 2015. Soil reinforcement capability of two legume species from plant morphological traits and mechanical properties. Curr. Sci. 108, 1340–1347.
Schanz, T., Vermeer, P.A., 1996. Angles of friction and dilatancy of sand. Géotechnique 46, 145–151. http://dx.doi.org/10.1680/geot.1996.46.1.145.
Schofield, A., Wroth, C.P., 1968. Critical State Soil Mechanics. McGraw Hill, Maidenhead.
Shibuya, S., Mitachi, T., Tamate, S., 1997. Interpretation of direct shear box testing of sands as quasi-simple shear. Géotechnique 47, 769–790. http://dx.doi.org/10.1680/geot.1997.47.4.769.
Shrestha, M.B., Horiuchi, M., Yamadera, Y., Miyazaki, T., 2000. A study on the adaptability mechanism of tree roots on steep slopes. In: The Supporting Roots of Trees and Woody Plants: Form, Function and Physiology. Springer Netherlands, Dordrecht, pp. 51–57. http://dx.doi.org/10.1007/978-94-017-3469-1_5.
Simon, A., Pollen, N., 2004. Assessing the relative timing and contribution of mechanical and hydrologic effects of vegetation on streambank stability erosion of streambanks. Riparian Veg. Fluv. Geomorphol. 125–139. http://dx.doi.org/10.1029/008WSA10.
Simoni, A., Houlsby, G.T., 2006. The direct shear strength and dilatancy of sand-gravel mixtures. Geotech. Geol. Eng. 24, 523–549. http://dx.doi.org/10.1007/s10706-004-5832-6.
Sonnenberg, R., Bransby, M.F., Hallett, P.D., Bengough, A.G., Mickovski, S.B., Davies, M.C.R., 2010. Centrifuge modelling of soil slopes reinforced with vegetation. Can. Geotech. J. 47, 1415–1430. http://dx.doi.org/10.1139/T10-037.
Springman, S.M., Teysseire, P., Jommi, C., 2003. Instabilities on moraine slopes induced by loss of suction: a case history. Géotechnique 53, 3–10. http://dx.doi.org/10.1680/geot.2003.53.1.3.
Terzaghi, K., Peck, R.B., Mesri, G., 1996. Soil Mechanics in Engineering Practice, Third Edition. Wiley-Interscience Publication, John Wiley and Sons, Inc.http://dx.doi.org/10.1016/S0013-7952(97)81919-9.
Ting, J.M., Torrence Martin, R., Ladd, C.C., 1983. Mechanisms of strength for frozen sand. J. Geotech. Eng. 109, 1286–1302. http://dx.doi.org/10.1061/(ASCE)0733-9410(1983)109:10(1286).
Veylon, G., Ghestem, M., Stokes, A., Bernard, A., 2015. Quantification of mechanical and hydric components of soil reinforcement by plant roots. Can. Geotech. J. (11), 1–11. http://dx.doi.org/10.1139/cgj-2014-0090.
Waldron, L.J., Dakessian, S., 1982. Effect of grass, legume, and tree roots on soil shearing resistance. Soil Sci. Soc. Am. J. 46, 894–899. http://dx.doi.org/10.2136/sssaj1982.03615995004600050002x.
White, W.A., 1949. Atterberg plastic limits of clay minerals. Am. Mineral. 34, 508–512.
Wu, P.-K., Matsushima, K., Tatsuoka, F., 2008. Effects of specimen size and some other factors on the strength and deformation of granular soil in direct shear tests. Geotech. Test. J. 31, 45–64. http://dx.doi.org/10.1520/GTJ100773.
Yildiz, A., Askarinejad, A., Graf, F., Rickli, C., Springman, S.M., 2015. Effects of roots and mycorrhizal fungi on the stability of slopes. In: Winter, M.G., Smith, D.M., Eldred, P.J.L., Toll, D.G. (Eds.), XVI ECSMGE Geotechnical Engineering for Infrastructure and Development. ICE Publishing, pp. 1693–1698. http://dx.doi.org/10.1680/ecsmge.60678.